Journal of Thermal Analysis and Calorimetry (2020) 139:3803–3816
https://doi.org/10.1007/s10973-019-08729-0

Simulating natural convection and entropy generation of a nanofluid in an inclined enclosure under an angled magnetic field with a circular fin and radiation effect

Rui Zhang[1] · Ali Ghasemi[2] · Azeez A. Barzinjy[3,4] · Maliheh Zareei[5] · Samir M. Hamad[6,7] · Masoud Afrand[8,9]

Received: 21 May 2019 / Accepted: 16 August 2019 / Published online: 3 September 2019

Abstract

Natural convection and radiation heat transfer of alumina (Al_2O_3)–water nanofluid are assessed in an enclosure under a magnetic field in different angles. The enclosure is a cavity at an angle of 45° with respect to the horizon, and a circular quadrant fin with the temperature T_h is placed at the bottom corner of the cavity. The right wall is considered at the temperature T_c, and the rest of the walls are defined as adiabatic. The governing equations of flow are solved using algebraic finite volume method and the SIMPLE algorithm. In this work, the entropy generation is also evaluated other than heat transfer. The parameters in the present work include Rayleigh and Hartmann numbers, radiation parameter, magnetic field angle, nanoparticles volume fraction and aspect ratio. The results indicate higher Nusselt number and entropy generation and a lower Bejan number for a higher Rayleigh number and a lower Hartmann number. Addition of 6% of the nanoparticles causes an increase of 10% in the heat transfer rate and 11% in the entropy generation in the absence of radiation. The addition of the radiation mechanism to the enclosure leads to an increase in the heat transfer rate and entropy generation. It is also demonstrated that the vertical magnetic field is more intense than the horizontal magnetic field in the enclosure. With an increase in the fin aspect ratio from 0.3 to 0.7, the rate of heat transfer and entropy generation increases by 36 and 27%, respectively.

Keywords Finite volume method · Nanofluid · Natural convection · Radiation · Magnetic field · Entropy generation

List of symbols

AR	Aspect ratio
B_0	Magnetic field strength
Be	Bejan number
C_p	Specific heat transfer coefficient (J kg^{-1} K^{-1})
G	Gravity (m s^{-2})

✉ Masoud Afrand
masoud.afrand@tdtu.edu.vn

Azeez A. Barzinjy
azeez.azeez@su.edu.krd

Samir M. Hamad
samir.hamad@soran.edu.iq

[1] School of Automotive and Transportation, Tianjin University of Technology and Education, Tianjin 300222, China

[2] Department of Mechanical Engineering, Amirkabir University of Technology (Tehran Polytechnic), Tehran, Iran

[3] Cihan Scientific Research Centre, Cihan University-Erbil, Erbil, Kurdistan Region, Iraq

[4] Physics Department, College of Education, Salahaddin University-Erbil, Erbil, Kurdistan Region, Iraq

[5] Department of Technical and Engineering, Zanjan Branch, Islamic Azad University, Zanjan, Iran

[6] Computer Department, Cihan University-Erbil, Erbil, Iraq

[7] Scintific Research Center, Soran University, Soran, Kurdistan Region, Iraq

[8] Laboratory of Magnetism and Magnetic Materials, Advanced Institute of Materials Science, Ton Duc Thang University, Ho Chi Minh City, Vietnam

[9] Faculty of Applied Sciences, Ton Duc Thang University, Ho Chi Minh City, Vietnam

h Convection heat transfer coefficient (W m^{-2} K^{-1})
Ha Hartmann number $\left(Ha = B_0 l\sqrt{\frac{\sigma_f}{\rho_f \vartheta_f}}\right)$
k Thermal conductivity (W m^{-1} K^{-1})
l Enclosure length (m)
L Non-dimensional enclosure length
Nu Nusselt number
Nu_Y Local Nusselt number
Nu_M Average Nusselt number
p Pressure (Pa)
P Non-dimensional pressure $\left(\bar{P}l^2/\rho_{nf}\alpha_f^2\right)$
Pr Prandtl number (ϑ_f/α_f)
r Radius of fin (m)
R Non-dimensional radius of fin
Rd Radiation parameter $\left(Rd = \frac{4\sigma_e T_e^3}{k_f \beta_R}\right)$
Ra Rayleigh number $(g\beta_f l^3(T_h - T_c)/\alpha_f \vartheta_f)$
S_{Total} Total entropy generation
T Temperature (K)
u, v Velocity components (m s^{-1})
U, V Velocity component $(U = ul/\alpha_f, V = vl/\alpha_f)$
x, y Cartesian coordinates in different directions (m)
X, Y Coordinates $(X = x/l, Y = y/l)$

Greek symbols

β Expansion coefficient (1 K^{-1})
α Fluid thermal diffusivity (m^2 s^{-1})
φ Volume fraction
ζ Irreversibility distribution ratio $\left(\zeta = \frac{\mu_{nf} T_0}{k_f}\left(\frac{\alpha_f}{L(T_h - T_C)}\right)^2\right)$
ω Angle of magnetic field (°)
θ Temperature
μ Dynamic viscosity (W m^{-1} K^{-1})
ϑ Kinematic viscosity (m^2 s^{-1})
ρ Density (kg m^{-3})
σ Electrical conductivity (Ω m)
γ Cavity angle (°)
ψ Stream function (m^2 s^{-1})
Ψ Dimensionless stream function

Subscripts

c Cold
h Hot
f Pure fluid
nf Nanofluid

Introduction

The closed enclosures are used in a variety of industries such as solar collectors, aerospace industries and petrochemicals. Natural convection is heat transfer mechanism in closed enclosures. Many researchers have already investigated convective heat transfer in the enclosures or tube due to high their application in industries [1–8]. Hence, the researchers attempt to enhance heat transfer in the cavities. Two suitable techniques that increase the heat transfer rate include the use of nanofluids and fins. Nanofluids have higher thermal conductivity than simple fluids lead to an increase in heat transfer [8–14]. The fins increase the heat transfer due to the enhancement of the heat exchange surface area [14–20]. Some researchers examined the heat transfer by adding nanofluid and fin to the enclosure simultaneously, e.g., Hashim et al. [21], Sheremet and Pop [22], Khanafer et al. [23] and Pordanjani et al. [24].

In most of the work, fins are rectangular and other geometries have been used rarely. Selimefendigil [25] used various parts of a circle as a fin to study the heat transfer rate in a trapezoid cavity. They used silicon oxide/water nanofluid and found that up to 16% enhancement in heat transfer is obtained by changing the fin geometry.

The enclosures are placed under the magnetic field in some applications in industries. The magnetic field is produced using an electric current located next to the enclosures. Therefore, studying the effect of magnetic field on natural convection heat transfer in the enclosures is necessary. Many researchers studied this problem [26–32]. The results of most papers show that increasing the magnetic field strength can reduce the heat transfer in the enclosures. Mehryan et al. [33] studied natural convection of iron oxide/water nanofluid in a closed cavity under a magnetic field. Pordanjani et al. [34] investigated natural convection of a nanofluid in a closed cavity under a magnetic field. They placed two squares fins inside the enclosure and examined their effect on the heat transfer rate. They presented that the heat transfer rate decreases with the Hartmann number.

Regarding the high energy consumption in human societies and the ending of fossil fuels, researchers have considered the efficiency of various devices. They used the second law of thermodynamics to examine the efficiency of various devices. They have tried to increase their efficiency by evaluating the entropy in engineering equipment. Entropy represents the degree of irreversibility in a process, and the entropy generation in various devices means an increase in energy losses that is undesirable [35, 36]. The researchers investigated the efficiency of enclosures by considering the entropy generation [27, 29, 37–40].

Pordanjani et al. [41] studied natural convection of alumina/water nanofluid in a closed cavity under a magnetic field under the boundary conditions of adiabatic upper and lower walls and a cold right wall. They applied different temperature profiles on the left wall to study heat transfer, entropy generation and Bejan number. They found that the entropy generation and the heat transfer rate increase with *Ra* and decrease with *Ha*. Radiation heat transfer is a mechanism of heat transfer that has many applications in heating industries, especially in solar collectors. This type of heat transfer has been less considered by the researchers. However, some researchers have investigated the radiation effect in the enclosures [42–49]. Tighchi et al. [50] investigated natural convection and radiation in a closed cavity. They put a thin fin on the left wall and examined the impact of the fin. Sobhani et al. [51] studied natural convection and radiation heat transfer in a square enclosure with a fined hot wall. The cavity had up and bottom insulated walls, right hot wall and left cold one. They studied the effect of fin and optimized it. Sheikholeslami and Seyednezhad [52] investigated natural convection and radiation heat transfer of ethylene glycol/iron oxide nanofluid in a closed enclosure and found that heat transfer increases by increasing the radiation parameter.

Natural convection and radiation have many applications in solar industries, such as solar collectors, water desalination, fruit dryers and water heaters. Also, since some of these devices are exposed to the magnetic field, the study of the magnetic field on the heat transfer rate is also necessary. The study of entropy generation is one of the suitable strategies to evaluate the efficiency of the system. In the present work, natural convection and entropy generation of alumina/water nanofluid in a square cavity under an angled magnetic field with volumetric radiation are investigated. There is a hot circular quadrant fin in the lower area of the left wall, which is the main objective of the present work. Since the simulation of this type of the geometries is difficult, the circular geometry is less considered. The effect of all the above-mentioned parameters and circular quadrant fin on the heat transfer and entropy generation is the unique contribution of the present work. In this paper, the effect of Rayleigh numbers, Hartmann number, radiation parameter, magnetic field angle and aspect ratio on heat transfer rate, entropy generation and Bejan number is investigated and the results are expressed in different diagrams and tables.

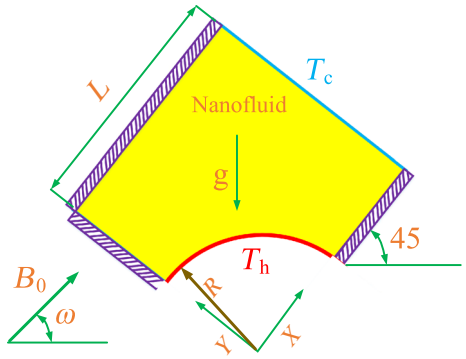

Fig. 1 A schematic of the problem under investigation

Problem setup

The studied geometry including an inclined two-dimensional cavity with alumina/water nanofluid is displayed in Fig. 1. The up, bottom and left walls are insulated. The right wall is at temperature T_c. A quarter circular fin with temperature T_h is placed at the bottom of the left wall. The enclosure has an angle of $\gamma = 45°$ with respect to the horizon. A magnetic field of B_0 and angle of ω is applied to the enclosure. The length and height of the cavity are equal to L, and a buoyancy force is formed due to the temperature difference. The buoyancy force is estimated by Boussinesq approximation.

Mathematical model

The non-dimensional governing equations for the fluid flow are as follows. These equations are written using the assumption of a steady and laminar flow and Newtonian and incompressible fluid. Also, volumetric forces are neglected except the gravitational and magnetic forces. The viscous dissipation is also ignored [34, 53]:

$$\frac{\mathrm{d}U}{\mathrm{d}X} + \frac{\partial V}{\partial Y} = 0 \tag{1}$$

$$\begin{aligned} U\frac{\partial U}{\partial X} + V\frac{\partial U}{\partial Y} &= -\frac{\partial P}{\partial X} + \frac{\mu_{\mathrm{nf}}}{\rho_{\mathrm{nf}}\alpha_{\mathrm{f}}}\left(\frac{\partial^2 U}{\partial X^2} + \frac{\partial^2 U}{\partial Y^2}\right) \\ &+ \frac{\rho_{\mathrm{f}}}{\rho_{\mathrm{nf}}}\frac{\sigma_{\mathrm{nf}}}{\sigma_{\mathrm{f}}} PrHa^2\left(V\sin\omega\cos\omega - U\sin^2\omega\right) \\ &+ \frac{\beta_{\mathrm{nf}}}{\beta_{\mathrm{f}}} RaPr\theta\sin\gamma \end{aligned} \tag{2}$$

$$U\frac{\partial V}{\partial X}+V\frac{\partial V}{\partial Y}=-\frac{\partial P}{\partial Y}+\frac{\mu_{\mathrm{nf}}}{\rho_{\mathrm{nf}}\alpha_{\mathrm{f}}}\left(\frac{\partial^2 V}{\partial X^2}+\frac{\partial^2 V}{\partial Y^2}\right)+\frac{\rho_{\mathrm{f}}}{\rho_{\mathrm{nf}}}\frac{\sigma_{\mathrm{nf}}}{\sigma_{\mathrm{f}}}PrHa^2\left(U\sin\omega\cos\omega-V\cos^2\omega\right)+\frac{\beta_{\mathrm{nf}}}{\beta_{\mathrm{f}}}RaPr\theta\cos\gamma \tag{3}$$

$$\left(U\frac{\partial\theta}{\partial X}+V\frac{\partial\theta}{\partial Y}\right)=\frac{\alpha_{\mathrm{nf}}}{\alpha_{\mathrm{f}}}\left(\frac{\partial^2\theta}{\partial X^2}+\frac{\partial^2\theta}{\partial Y^2}\right)+\frac{4}{3}\frac{k_{\mathrm{nf}}/k_{\mathrm{f}}}{(\rho C_{\mathrm{P}})_{\mathrm{nf}}/(\rho C_{\mathrm{P}})_{\mathrm{f}}}\left(\frac{k_{\mathrm{nf}}}{k_{\mathrm{f}}}\right)^{-1}Rd\frac{\partial^2\theta}{\partial Y^2} \tag{4}$$

$$S_{\mathrm{gen}}=\frac{k_{\mathrm{nf}}}{k_{\mathrm{f}}}\left(\left(\frac{\partial\theta}{\partial X}\right)^2+\left(\frac{\partial\theta}{\partial Y}\right)^2\right)+\zeta\left\{2\left[\left(\frac{\partial U}{\partial X}\right)^2+\left(\frac{\partial V}{\partial Y}\right)^2\right]+\left(\frac{\partial U}{\partial Y}+\frac{\partial V}{\partial X}\right)^2\right\}+\zeta\frac{\sigma_{\mathrm{nf}}}{\sigma_{\mathrm{f}}}\frac{\mu_{\mathrm{f}}}{\mu_{\mathrm{nf}}}Ha^2(U\sin\omega-V\cos\omega)^2 \tag{5}$$

The following parameters are used to non-dimensionalize the governing equations and the boundary conditions where the definitions of Rayleigh, Hartman, Bejan and Prandtl numbers, radiation parameter and entropy generation are expressed.

$$X=\frac{x}{l},\quad Y=\frac{y}{l},\quad U=\frac{ul}{\alpha_{\mathrm{f}}},\quad V=\frac{vl}{\alpha_{\mathrm{f}}},\quad P=\frac{\bar{P}l^2}{\rho_{\mathrm{nf}}\alpha_{\mathrm{f}}^2},$$
$$\theta=\frac{T-T_{\mathrm{c}}}{T_{\mathrm{h}}-T_{\mathrm{c}}},\quad L=\frac{l}{l},\quad R=\frac{r}{l}$$
$$Pr=\frac{\vartheta_{\mathrm{f}}}{\alpha_{\mathrm{f}}},\quad Be=\frac{S_{\mathrm{gen,T}}}{S_{\mathrm{Total}}},\quad Ra=\frac{g\beta_{\mathrm{f}}l^3(T_{\mathrm{h}}-T_{\mathrm{c}})}{\alpha_{\mathrm{f}}\vartheta_{\mathrm{f}}},$$
$$Ha=B_0l\sqrt{\frac{\sigma_{\mathrm{f}}}{\rho_{\mathrm{f}}\vartheta_{\mathrm{f}}}},\quad Rd=\frac{4\sigma_{\mathrm{e}}T_{\mathrm{c}}^3}{k_{\mathrm{f}}\beta_{\mathrm{R}}}$$
$$\zeta=\frac{\mu_{\mathrm{nf}}T_0}{k_{\mathrm{f}}}\left(\frac{\alpha_{\mathrm{f}}}{L(T_{\mathrm{h}}-T_{\mathrm{C}})}\right)^2 \tag{6}$$

By considering radiation heat transfer, the following term is added to the energy equation:

$$-\frac{1}{\rho C_{\mathrm{p}}}\frac{\partial q_{\mathrm{r}}}{\partial y} \tag{7}$$

There are various methods to solve the above equation. One of these methods is the Russland method. In this method, the following equation is used instead of the value expressed in Eq. (7):

$$q_{\mathrm{r}}=-\frac{4}{3}\frac{\sigma_{\mathrm{e}}}{\beta_{\mathrm{R}}}\frac{\partial T^4}{\partial y},\quad T^4=4T_{\mathrm{c}}^3T-3T_{\mathrm{c}}^4 \tag{8}$$

Table 1 Non-dimensional governing boundary conditions

Left wall	$\begin{cases}0\le Y\le 1\\ X=0\end{cases}$	$U=V=0$	$\frac{\partial\theta}{\partial x}=0$
Right wall	$\begin{cases}0\le Y\le 1\\ X=1\end{cases}$	$U=V=0$	$\theta=0$
Up wall	$\begin{cases}0\le X\le 1\\ Y=1\end{cases}$	$U=V=0$	$\frac{\partial\theta}{\partial y}=0$
Bottom wall	$\begin{cases}0\le X\le 1\\ Y=0\end{cases}$	$U=V=0$	$\frac{\partial\theta}{\partial y}=0$
Fin	$X^2+Y^2=R^2$	$U=V=0$	$\theta=1$

Non-dimensional boundary conditions are presented as follows in Table 1.

The properties of nanofluid including σ, ρ, β, c_{p} and α are calculated as:

$$\sigma_{\mathrm{nf}}=(1-\varphi)\sigma_{\mathrm{f}}+\varphi\sigma_{\mathrm{s}} \tag{9}$$
$$\rho_{\mathrm{nf}}=(1-\varphi)\rho_{\mathrm{f}}+\varphi\rho_{\mathrm{s}} \tag{10}$$
$$(\rho\beta)_{\mathrm{nf}}=(1-\varphi)(\rho\beta)_{\mathrm{f}}+\varphi(\rho\beta)_{\mathrm{p}} \tag{11}$$
$$(\rho c_{\mathrm{p}})_{\mathrm{nf}}=(1-\varphi)(\rho c_{\mathrm{p}})_{\mathrm{f}}+\varphi(\rho c_{\mathrm{p}})_{\mathrm{s}} \tag{12}$$
$$\alpha_{\mathrm{nf}}=\frac{k_{\mathrm{nf}}}{(\rho c_{\mathrm{p}})_{\mathrm{nf}}} \tag{13}$$

Most of the numerical correlations for thermal conductivity and viscosity of nanofluid depend only on the volume fraction and do not depend on the temperature. However, since they depend on both the temperature and nanoparticles volume fraction, the Vajjha model [54] is used in the present work, which also considers the influence of Brownian diffusion. Brownian motion is one of the dominant physical phenomena on nanofluids, and the simulations lead to errors if this motion is not considered.

According to Vajjha model [54], the thermal conductivity coefficient involves thermal conductivity of stationary and Brownian motion, where k_{Static} is obtained from Maxwell relation [55]. The nanofluid thermal conductivity is determined as:

$$k_{\mathrm{nf}}=k_{\mathrm{Static}}+k_{\mathrm{Brownian}}=\frac{k_{\mathrm{s}}+2k_{\mathrm{f}}-2(k_{\mathrm{f}}-k_{\mathrm{s}})}{k_{\mathrm{s}}+2k_{\mathrm{f}}+(k_{\mathrm{f}}-k_{\mathrm{s}})\varphi}k_{\mathrm{f}}+5\times10^4\beta\varphi\rho_{\mathrm{f}}(C_{\mathrm{p}})_{\mathrm{f}}\sqrt{\frac{kT}{\rho_{\mathrm{s}}d_{\mathrm{s}}}}f(T,\varphi) \tag{14}$$

Note that the subscripts f and s refer to water and Al_2O_3, respectively, and the properties are presented in Table 2.

There are static and Brownian values for the viscosity that the term μ_{Static} is derived from the Brinkman relationship [56]. Finally, the viscosity relation is written as Eq. 15:

Table 2 Thermophysical properties of Al_2O_3 and water [54]

	C_P/J kg^{-1} K^{-1}	k/W m^{-1} K^{-1}	ρ/kg m^{-3}	μ/kg m^{-1} s^{-1}	σ/Ω m^{-1}	d_S/nm
Water	4179	0.613	997.1	0.001	0.05	–
Al_2O_3	765	40	3970	–	10^{-12}	47

$$\mu_{nf} = \mu_{Static} + \mu_{Brownian} = \frac{\mu_f}{(1-\varphi)^{2.5}} + 5\times 10^4 \beta\varphi\rho_f (C_p)_f \frac{\mu_f}{k_f Pr}\sqrt{\frac{k_b T}{\rho_p d_s}} f(T\varphi) \quad (15)$$

where [56]:

$$f(T\varphi) = \left(2.8217\times 10^{-2}\varphi + 3.917\times 10^{-3}\right)\left(\frac{T}{T_0}\right) + \left(-3.0669\times 10^{-2}\varphi - 3.91123\times 10^{-3}\right) \quad (16)$$

$$\beta = 8.4407(100\varphi)^{-1.07304} \quad (17)$$

By integrating the total solution range, S_{Total} and average Bejan number are obtained:

$$S_{Total} = \int S_{gen} d\Omega = \iint_0^1 S_{gen} dX dY \quad (18)$$

$$B_{Ave} = \iint_0^1 Be dX dY \quad (19)$$

Nu_Y is used to determine the heat transfer on the cold wall calculated as:

$$Nu_Y = \frac{hL}{k_f} + Nu_{Rd} \quad (20)$$

where h is defined as:

$$h = \frac{q_\omega}{T_h - T_c} \quad (21)$$

The heat flux is also expressed by Eq. (22):

$$q_\omega = k_{nf}\left(\frac{\partial T}{\partial X}\right) \quad (22)$$

Considering the presence of radiation in the enclosure, Nu_Y is ultimately calculated as:

$$Nu = -\frac{k_{nf}}{k_f}\left(\frac{\partial\theta}{\partial X}\right) + \frac{4}{3}Rd\left(\frac{\partial\theta}{\partial X}\right) = \frac{k_{nf}}{k_f}\left(1 + \frac{4}{3}Rd\frac{k_f}{k_{nf}}\right)\frac{\partial\theta}{\partial X} \quad (23)$$

Nu_M is obtained by integrating above equation over the cavity cold wall as:

$$Nu_M = \frac{1}{L}\int_0^L Nu_{(x=0,1)} dY = -\frac{1}{L}\frac{k_{nf}}{k_f}\int_0^L \left(\frac{\partial\theta}{\partial X}\right)_{(x=0,1)} dY \quad (24)$$

Numerical method

Equations 1–5 and boundary conditions presented in Table 1 are solved using FVM. The domain is discretized using SIMPLE algorithm by a staggered grid which causes a more simple calculating flow on the control volume and also pressure calculation due to the known velocity of the surfaces. The full details are given in Ref. [57]. Finally, the code is implemented using FORTRAN software with the convergence criteria given as:

$$\Phi = \sum_J \sum_I \left|\frac{\varphi^{n+1} - \varphi^n}{\varphi^{n+1}}\right| \le 10^{-8} \quad (25)$$

To solve the equations, a 16 GB DDR4 RAM with a CPU 3.6 was used. Due to the fineness of the mesh, the approximate time of each hip lasts 40 min. In fact, the mesh selection was based on the evaluation of the grid independency. However, the running time of the code was dependent on cases such as the activation of radiation heat transfer, Rayleigh and Hartmann number. Regarding Fig. 2, uniform gridding for enclosure was also used. In order to create the domain of the simulated model, as shown in Fig. 2, a square box was considered. Circumference quadrant block is assumed to be zigzag. Cells that are outside the range of the quadric circle have been disabled.

Validation

For the code validation, the present results are compared with four numerical and experimental studies. First, the experimental results of Krane and Jessee [58] are considered. They investigated air flow in a cavity. The vertical velocity profile is plotted in Fig. 3 showing the very good agreement of the present results with the experimental ones.

The second comparison is performed with Ghasemi et al. [59]. The enclosure is under the magnetic field. In Table 3, Nu_M is compared for $Ra = 10^5$ and $Ha = 60$ showing a good agreement.

The third comparison is done using the results of Alnaqi et al. [42]. The results are presented in Table 4 for three different radiation parameters showing a good agreement.

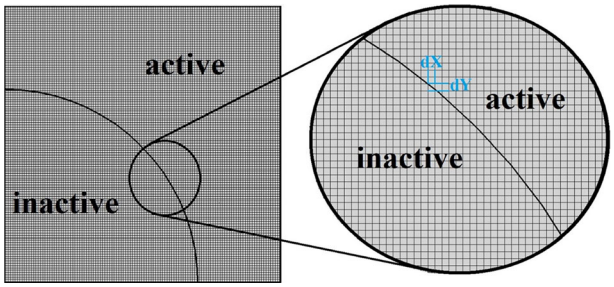

Fig. 2 The spatial discretization of the computational domain of the square box

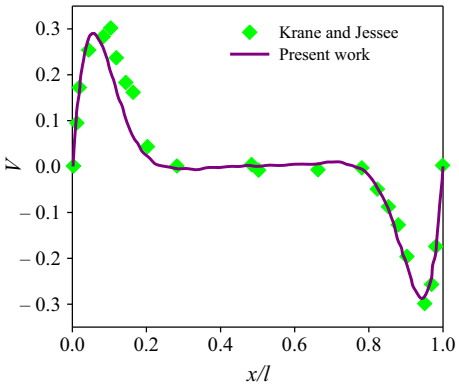

Fig. 3 The profile of vertical velocity component: comparison between the present results and those of Krane and Jessee [58]

Table 3 Comparison between the Nu_M from the present simulations and the one reported by Ghasemi et al. [59] for different volume fractions of nanoparticles

φ	0.0	0.02	0.04	0.06
Present work	1.927	1.915	1.907	1.809
Ghasemi et al. [59]	1.851	1.831	1.815	1.806
Error/%	4.1	4.5	5.0	0.1

Table 4 Entropy generation for different radiation parameters: a comparison between the present results and the results of Alnaqi et al. [42]

	$Rd = 0$	$Rd = 1$	$Rd = 2$
S_{Total}			
Alnaqi et al. [42]	74.02	79.53	82.30
Present work	76.20	80.30	83.60
$\%\left(\frac{S_{\text{Total}} - S_{\text{Total, Alnaqietal.[42]}}}{S_{\text{Total}}} * 100\right)$			
Error (%)	3%	1%	0.3%

Grid resolution test

For the grid independency assessment, the mean Nusselt number and entropy generation are calculated for $Ha = 20$, $\varphi = 0.03$, $Y = 0.6$, $AR = 0.5$, $Rd = 1$, $\omega = 45°$ and $Ra = 10^5$ for different grid resolutions (Table 5). It can be seen that the grid resolution of 120 × 120 is enough for present simulations and further increase does not change the results.

Results and discussion

Variations of radiation parameter

Figure 4 illustrates the stream, isothermal and isentropic lines for $Ra = 10^5, Ha = 20, \omega = 0, \varphi = 0.03, \text{AR} = 0.5$ for different radiation parameters. A clockwise vortex is generated in the cavity due to the buoyancy effect. The fluid is cooled in the vicinity of the cold wall, resulting in a reduction in its molecular momentum, and as a result, its molecules become closer together. Hence, the fluid density increases in this area. The heavy fluid moves down and replaced by low-density fluid. The same phenomenon happens close to the fin: the fluid is heated in the vicinity of the fin leads to a reduction in its density. The heated fluid moves upward. With the continuation of these movements of the fluid mass, a vortex is formed in the cavity results in replacing the hot and cold fluids. This difference in density creates a force called the buoyancy force. The higher the density difference, the larger the buoyancy force results in a faster movement of the vortex in the enclosure. By enhancing *Rd*, the maximum amount of the stream function increases. This value indicates the strength of the vortex. Larger stream function causes the vortex circulates faster in the cavity. When the radiation is considered in the enclosure, another heat transfer mechanism is added into the cavity leads to a higher heat transfer between the constant temperature walls and the fluid. This means that the fluid is hotter near the hot fin and colder near the cold wall. Therefore, the density changes also increase. For a higher radiation parameter, the curvature of the isothermal lines is slightly increased. The main heat transfer mechanism can be realized from the curvature of the isothermal lines. Regular lines with low curvature mean conduction heat transfer, and irregular lines with large curvature exhibit convection. Enhancing the curvature of isothermal lines means a higher heat transfer due to an increase in the vortex velocity by increasing *Rd*. For a higher vortex velocity, natural convection increases while conduction is weakened. Since the increase in natural convection leads to higher heat transfer rate, the addition of radiation to the enclosure can also increase the rate of heat transfer. The density of isentropic lines slightly rises. S_{Total} includes the thermal entropy generation depending on the temperature gradient, entropy generation due to viscous dissipation depending on the velocity gradient and also due to the

Table 5 Grid resolution test

Grid	60 × 60	80 × 80	100 × 100	120 × 120	140 × 140	160 × 160
Nu_{ave}	4.109	4.146	4.193	4.199	4.198	4.198
%ErrNu_{ave}	2.1	1.2	0.1	0	0	0
$\lvert\Psi_{max}\rvert$	10.643	10.897	11.001	11.139	11.139	11.138
%Err$\lvert\Psi_{max}\rvert$	4.4	2.1	1.2	0	0	0
S_{Total}	6.137	6.356	6.401	6.417	6.417	6.416
%ErrS_{Total}	4.3	0.9	0.2	0	0	0

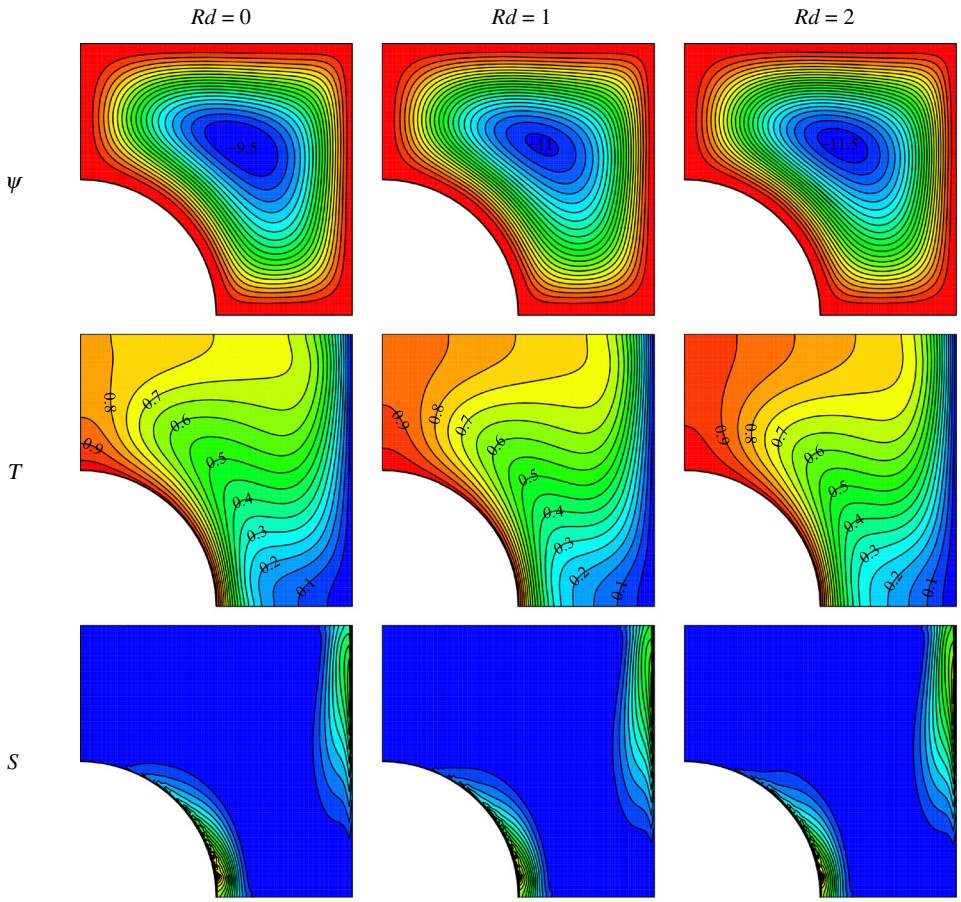

Fig. 4 Streamlines, isotherms and isentropic lines for $Ra = 10^5$, $Ha = 20$, $\omega = 0$, $\varphi = 0.03$, AR = 0.5 and different Rd

magnetic field depending on the difference in velocities in the horizontal and vertical directions. An increase in the radiation parameter leads to an increase in the fluid velocity of the enclosure results in an increase in the velocity gradient and entropy generation. This also results in the enhancement of S_{Total}, which is concluded from the relative increase in the density of isentropic lines.

Nu_Y calculated on the cavity cold wall is displayed in Fig. 5 for $Ra = 10^5, Ha = 20, \omega = 0, \varphi = 0.03, \text{AR} = 0.5$ and various radiation parameters. The local rate of heat transfer enhances the radiation in the enclosure. For a constant Rd, the heat transfer rate increases from the bottom to the upper parts of the hot wall based on the direction of the vortex. The hot fluid collides with the cold wall in its upper part for the first time. Therefore, the temperature gradient is high in this region, which causes a higher rate of heat transfer. By the fluid movement across the cold wall and losing its temperature, the temperature gradient also reduces. Hence, the temperature gradient decreases sharply in the lower parts of the wall and the amount of heat transfer is also negligible. Adding radiation to the enclosure enhance the rate of heat transfer. For a higher the rate of radiation heat transfer, the Nusselt number increases.

In Table 6, the variations of Nu_M calculated on the cold wall and S_{Total} are displayed for $Ra = 10^5, Ha = 20, \omega = 0.03, AR = 0.5$ for different nanoparticles volume fractions and two radiation parameters. Nu_M increases with a higher nanoparticles volume fraction. Thermal conductivity enhances for a higher nanoparticles volume fraction. So, higher heat transfer occurs between the fluid and the constant temperature walls. For a higher nanoparticles volume fraction, the thermal conductivity and the heat transfer rate enhance. Entropy generation is related to the nanoparticles volume fraction, and thermal conductivity increases with the volume fraction. Thermal conductivity coefficient of the nanofluid is effective in thermal entropy which increases with the thermal conductivity coefficient. In addition, an increase in the thermal conductivity causes higher heat transfer between the fluid and constant temperature walls leads to an increase in the density gradient in the enclosure. Consequently, the buoyancy force and the vortex velocity enhance in the enclosure, which ultimately leads to velocity gradient. Entropy generation due to viscous dissipation increases by increasing the velocity gradient. The Nusselt number also rises significantly by increasing the radiation parameter. This increase is due to the addition of another heat transfer mechanism to the cavity, which increases the heat transfer rate. An increase in the radiation parameter leads to an increase in entropy generation, but the increase is very low compared to the Nusselt number. The vortex velocity boosts for a higher Rd leads to the enhancement of velocity gradient, and viscous dissipation entropy generation results in a higher S_{Total}.

Variations of magnetic field angle

Figure 6 shows the streamlines, isotherms and isentropic lines for $Ra = 10^5, Ha = 20, Rd = 1, \varphi = 0.03, AR = 0.5$ and different magnetic angles. The strength of the vortex initially decreases and then increases by increasing ω. In general, the magnetic field induces the Lorentz force into the fluid. This force reduces the flow rate of the fluid in the cavity and reduces the buoyancy force. Changes ω change the angle of the Lorentz force. It can help the formation of the vortex or prevent its formation. Since the inclination angle and ω are 45°, the Lorentz force prevents the formation of the vortex and reduces its strength. This force is less opposed to the formation of the vortex in the horizontal and vertical enclosures, which is why the velocity is reduced less. At the angles of the magnetic field that the vortex is stronger, the isothermal lines are denser and more curved. This is due to the faster velocity of the vortex leads to higher natural convection. Furthermore, the density of isentropic lines increases with the strength of the vortex. This means that the entropy generation is higher due to higher velocity gradient and faster vortex velocity in the cavity results in a higher entropy generation due to viscous dissipation resulting in a high S_{Total}.

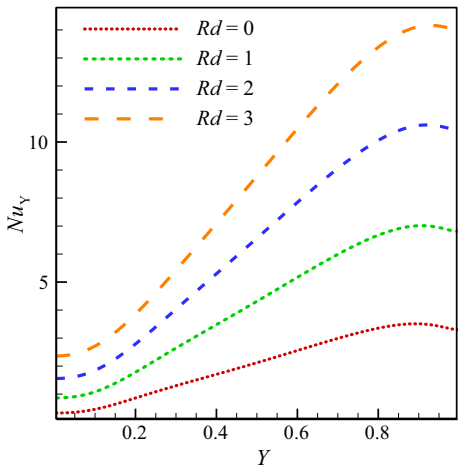

Fig. 5 Cold wall Nu_Y for $Ra = 10^5, Ha = 20, \omega = 0, \varphi = 0.03$, AR = 0.5 and different Rd

Table 6 Variations of cold wall Nu_M and S_{Total} for $Ra = 10^5$, $Ha = 20$, $\omega = 0.03$, AR = 0.5 and different volume fractions of nanoparticles and two radiation parameters

	$\varphi = 0.00$	$\varphi = 0.03$	$\varphi = 0.06$
$Rd = 0$			
Nu_M	1.99	2.06	2.19
$\%\left(\frac{Nu_\varphi - Nu_{\varphi=0}}{Nu_{\varphi=0}}\right)$	0.0	3.5	10
S_{total}	5.85	6.09	6.50
$\%\left(\frac{S_\varphi - S_{\varphi=0}}{S_{\varphi=0}}\right)$	0.0	4.1	11.1
$Rd = 2$			
Nu_M	6.41	6.40	6.38
$\%\left(\frac{Nu_{Rd} - Nu_{Rd=0}}{Nu_{Rd=0}}\right)$	222	210	191
S_{total}	6.33	6.57	6.96
$\%\left(\frac{S_{Rd} - S_{Rd=0}}{S_{Rd=0}}\right)$	8.2	7.08	7.0

In Fig. 7, cold wall Nu_Y is plotted for $Ra = 10^5, Ha = 20, Rd = 1, \varphi = 0.03, AR = 0.5$ and different ω. At a constant ω, Nu_Y increases for a higher height. This is due to the higher temperature gradient in the upper areas of the cavity. In these areas, the hot fluid collides with the cold wall for the first time results in a higher heat transfer. At the angles of the magnetic field equal to 0° and 90°, the Lorentz force causes the fluid to collide more with the cold wall in the middle section of the wall. Hence, the temperature gradient and consequently the Nusselt number increase in these regions. In these situations, the Lorentz force does not allow the motion of the fluid to the upper section of the enclosure. Therefore, the temperature gradient decreases. This can be observed from the figure.

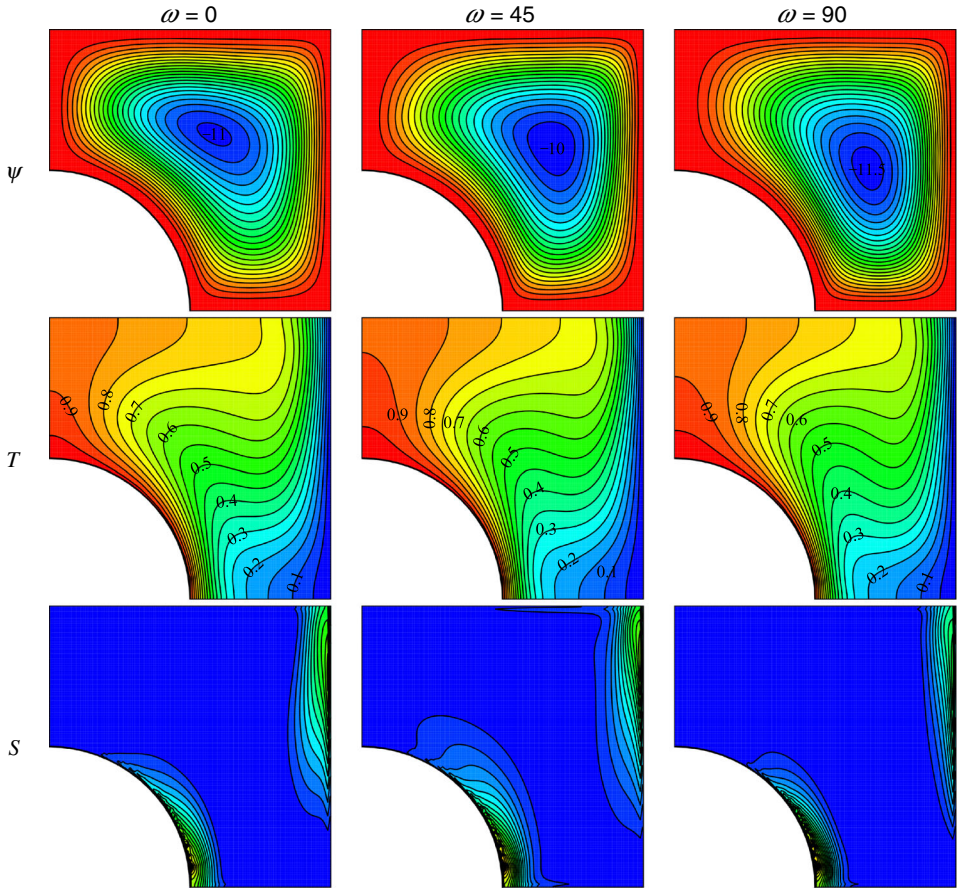

Fig. 6 Streamlines, isotherms and isentropic lines for $Ra = 10^5,\ Ha = 20,\ Rd = 1,\ \varphi = 0.03,\ \mathrm{AR} = 0.5$ and different magnetic angles

Variations of aspect ratio

In Fig. 8, the streamlines, isotherms and isentropic lines for $Ra = 10^5, Ha = 20, Rd = 1, \omega = 0, \varphi = 0.03$ and different ARs are shown. The maximum stream function value decreases by increasing the size of the fin. Two phenomena occur by increasing the AR: first, the interior space of the cavity to form the vortex becomes smaller. Consequently, the flow fluid velocity decreases and the strength of the vortex decreases. This is clearly observed from the flow field. On the other hand, the size of the hot wall increases with AR. As a result, the fluid remains more in the vicinity of the hot wall and becomes hotter, resulting in higher density differences in the enclosure and larger buoyancy force. Since the weakening of the vortex is more than its strength, its strength decreases by increasing AR. As AR increases, the density of isothermal lines near the cold wall and the hot fin increases. This indicates that the temperature gradient increases in these areas causing a higher heat transfer rate. It also shows that the curvature of lines becomes smaller and their regularity increases. The shape of the lines represents the heat transfer mechanism. Thus, the main heat transfer mechanism changes from convection to conduction by increasing the size of the fin. The density of isentropic lines increases initially and then decreases. The temperature increases and the velocity gradient decreases for a higher fin size. This means that thermal entropy generation increases and the entropy generation due to viscous dissipation decreases. Hence, S_{Total} increases or decreases due to velocity and temperature gradients. For the initial increase in AR, the increase in the temperature gradient is dominant and S_{Total} increases. After an initial increase in AR, S_{Total} decreases.

In Fig. 9, cold wall Nu_{Y} is plotted for $Ra = 10^5, Ha = 20, Rd = 1, \omega = 0, \varphi = 0.03$ and different ARs. The heat transfer rate increases in the upper section of the cold wall by enlarging AR. The density of the isothermal lines increases and the flow velocity decreases in the cavity with AR. As the flow velocity decreases in the enclosure, the heat transfer mechanism changes from convection to conduction. Since conduction heat transfer depends on the distance between hot and cold sources, the conduction heat transfer increases as the hot fin approaches to the cold wall. This position makes the Nusselt number increases. In the lower part of the wall, lower penetration of the flow causes a weak heat transfer by increasing AR. Therefore, it has

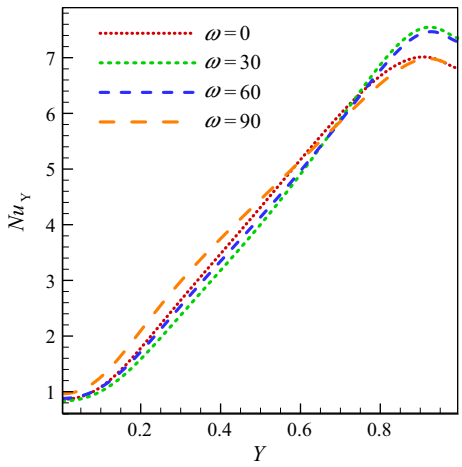

Fig. 7 Nu_Y calculated on the cold wall for $Ra = 10^5$, $Ha = 20$, $Rd = 1$, $\varphi = 0.03$, AR $= 0.5$ and different angles of the magnetic field

been seen that Nu_Y decreases in the middle part of the wall for a high AR.

Figure 9 shows the cold wall Nu_Y for $Ra = 10^5, Ha = 20, Rd = 1, \omega = 0, \varphi = 0.03$ and different ARs.

In Table 7, cold wall Nu_M is shown for $Ra = 10^5, Ha = 20, Rd = 1, \omega = 0, \varphi = 0.03$ and different ARs. The heat transfer rate enhances by increasing AR of the cavity due to two reasons: (1) the heat source is larger with the increase in the fin. Hence, the fluid is heating in a larger space, and it can become hotter results in a higher temperature gradient and therefore higher heat transfer rate. (2) Since the conduction heat transfer is one of heat transfer mechanisms, for a higher AR, higher conduction heat transfer is occurred. So, the conduction heat transfer and Nu_M increase by decreasing the distance between the heat source and the cold wall. The heat transfer rate reduces for a higher Ha and reduces the vortex velocity. The Lorentz force prevents the velocity of the vortex by increasing the magnetic field. As a result, the velocity decreases in the cavity. This eventually leads to a reduction in the heat transfer rate. As shown, Nu_M decreases with Ha.

In Table 8, S_{Total} is displayed for $Ra = 10^5, Ha = 20, Rd = 1, \omega = 0, \varphi = 0.03$ and different ARs. Entropy generation increases for a higher size of the fin from 0.3 to 0.5. In this case, the heat exchanger surface increases between the fluid and the fin and the fluid becomes warmer due to increasing the size of the hot wall. This increases the temperature gradient near the cold wall results in a higher thermal entropy. On the other hand, the space for the formation of the vortex is reduced and the strength and vortex velocity decrease with AR. Consequently, the velocity gradient in the cavity decreases. The entropy due to viscous dissipation decreases by decreasing the velocity gradient. As the size of the fin increases, thermal entropy generation increases and the entropy due to viscous dissipation decreases. For smaller sizes of the fin, the enhancement of thermal entropy is more than that of the entropy due to viscous dissipation, resulting in an increase in S_{Total}. But for large fins, the entropy due to viscous dissipation decreases significantly and leads to a reduction in S_{Total} due to smaller space for the formation of the vortex. The velocity and temperature gradients are reduced by increasing Ha and decreasing the flow rate of the fluid in the enclosure. Hence, thermal entropy and the entropy due to viscous dissipation decrease leading to a reduction in the S_{Total}.

Variations of Hartmann and Rayleigh numbers

In Table 9, Nu_M calculated on the cold wall is plotted for $Rd = 1, \omega = 0, \varphi = 0.03, \text{AR} = 0.5$ and different Ha and Ra. The heat transfer rate boosts with Ra. Ra represents the buoyancy force. The vortex velocity increases and the hydrodynamic boundary layer thickness formed on the walls decreases by increasing the buoyancy force. The thermal boundary layer thickness decreases by reducing the hydrodynamic boundary layer thickness. As a result, the temperature gradients increase near the walls and the heat transfer rate increases. As Ha increases, Lorentz force becomes stronger. The Lorentz force prevents the movement of the vortex, and thus, the velocity of the vortex decreases. Finally, the heat transfer rate is also reduced by decreasing the vortex velocity.

In Table 10, S_{Total} calculated for $Rd = 1, \omega = 0, \varphi = 0.03, \text{AR} = 0.5$ and different Ha and Ra is shown. As Ra, the velocity of the vortex increases. The temperature gradient also increases as described above. The entropy due to viscous dissipation and thermal entropy increase by increasing the velocity and temperature gradients, respectively. S_{Total} increases by increasing the entropy due to viscous dissipation and thermal entropy. The entropy due to viscous dissipation and thermal entropy decrease by increasing Ha leading to a reduction in the S_{Total}. This is clearly observed from the figure. It is noteworthy that the entropy of the magnetic field depends on Ha and increases with increasing Ha. However, since Ha is multiplied by the velocity difference, increasing Ha causes a reduction in the fluid velocity. As a result, increasing Ha does not change the entropy generation due to the magnetic field. In general, the entropy due to the magnetic field is smaller than the other two entropy parameters. The changes in S_{Total} are

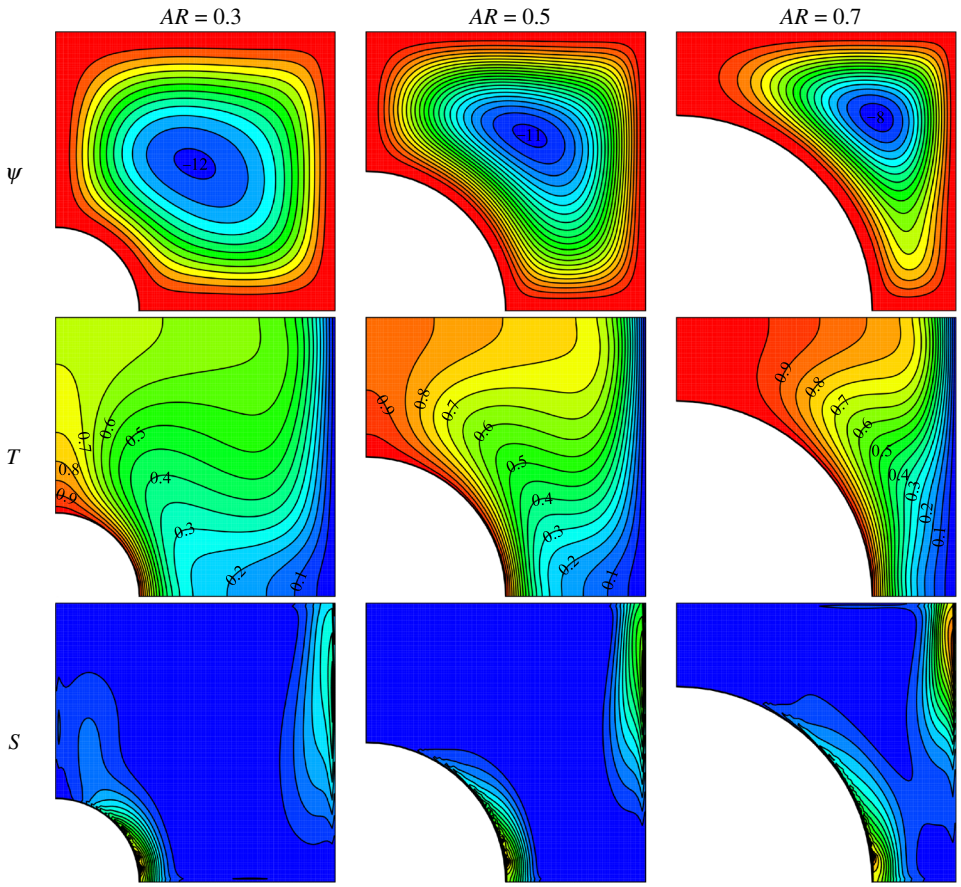

Fig. 8 Streamlines, isotherms and isentropic lines for $Ra = 10^5, Ha = 20, Rd = 1, \omega = 0, \varphi = 0.03$ and different AR

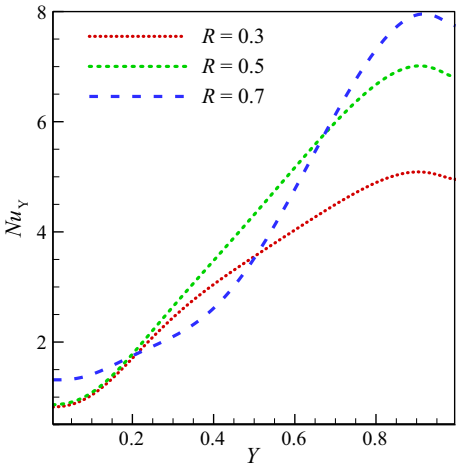

Fig. 9 Cold wall Nu_Y for $Ra = 10^5$, $Ha = 20$, $Rd = 1$, $\omega = 0$, $\varphi = 0.03$ and different AR

dependent on thermal entropy and entropy due to viscous dissipation.

Table 11 shows the Bejan number for $Rd = 1, \omega = 0, \varphi = 0.03, \mathrm{AR} = 0.5$ and different Ha and Ra. Be is defined as the ratio of thermal entropy generation and S_{Total}. As Ra increases, all components of S_{Total} increase.

Table 7 Cold wall Nu_{M} in terms of AR for $Ra = 10^5, Ha = 20, Rd = 1, \omega = 0, \varphi = 0.03$

	Ha = 00	Ha = 20	Ha = 40
AR = 0.3	3.73	3.31	2.46
AR = 0.5	4.89	4.19	2.93
AR = 0.7	5.08	4.20	3.25

Table 8 S_{Total} for $Ra = 10^5$, $Ha = 20$, $Rd = 1$, $\omega = 0$, $\varphi = 0.03$ and different AR

	Ha = 00	Ha = 20	Ha = 40
AR = 0.3	6.04	5.51	4.11
AR = 0.5	7.28	6.41	4.40
AR = 0.7	6.94	5.72	4.14

This means that S_{Total} increases greatly. This increase is significant compared to the increase in thermal entropy. Since the rate of enhancement of S_{Total} is greater than that

Table 9 Nu_M calculated on the cold wall for $Rd = 1$, $\omega = 0$, $\varphi = 0.03$, $AR = 0.5$ and different Ha and Ra

	Ha = 00	Ha = 20	Ha = 40
$Ra = 10^3$	1.62	2.38	4.89
$Ra = 10^4$	1.61	2.74	4.19
$Ra = 10^5$	1.61	1.61	2.93

Table 10 S_{Total} for $Rd = 1$, $\omega = 0$, $\varphi = 0.03$, AR = 0.5 and different Ha and Ra

	Ha = 00	Ha = 20	Ha = 40
$Ra = 10^3$	1.66	2.47	7.28
$Ra = 10^4$	1.65	1.83	6.41
$Ra = 10^5$	1.64	1.68	4.43

Table 11 The Bejan number for $Rd = 1$, $\omega = 0$, $\varphi = 0.03$, AR = 0.5 and different Ha and Ra

	Ha = 00	Ha = 20	Ha = 40
$Ra = 10^3$	0.99	0.90	0.53
$Ra = 10^4$	0.99	0.95	0.53
$Ra = 10^5$	0.99	0.98	0.61

of thermal entropy, Be is reduced. This is evident from the figure. As Ha increases, Be increases. The reason is that the rate of reduction in the total entropy is higher than that in thermal entropy. Hence, Be increases. As Ha increases, S_{Total} decreases dramatically results in a higher Be.

Conclusions

Natural convection and radiation heat transfer of a nanofluid including alumina and water in an enclosure under an angled magnetic field were numerically investigated. A circular quadrant fin was placed inside the enclosure and the influence of fin on the heat transfer rate, entropy generation and the Bejan number and the following results were obtained:

- By adding 6% of the nanoparticles to the base fluid in the absence of the radiation parameter, due to the increase in the thermal conductivity of the nanofluid, the heat transfer rate and the entropy generation increased by 10% and 11%, respectively.
- The heat transfer rate increases 3.2 times, and the entropy generation boosts by 8.2% by increasing the radiation precursor from 0 to 2.
- Increasing the size of the fin from 0.3 to 0.7 results in 36 and 27% increase in the Nusselt number and entropy generation, respectively.
- Increasing the Rayleigh number led to an increase in the heat transfer rate and total entropy generation, but reduced Bejan number decreased.
- Unlike the Rayleigh number effect, increasing the Hartmann number reduced the heat transfer rate and entropy generation, while increased the Bejan number.

Acknowledgements This research is partially supported by the National Key Research and Development Program (2016YFB0100903), the National Science Foundation of China (61503284), the Tianjin Key R&D Program (18YFZCGX00380), and Tianjin Science and Technology Major Project for Artificial Intelligence (17ZXRGGX00070).

References

1. Aghakhani S, Ghasemi B, Hajatzadeh Pordanjani A, Wongwises S, Afrand M. Effect of replacing nanofluid instead of water on heat transfer in a channel with extended surfaces under a magnetic field. Int J Numer Methods Heat Fluid Flow. 2019;29:1249–71.
2. Shahsavani E, Afrand M, Kalbasi R. Using experimental data to estimate the heat transfer and pressure drop of non-Newtonian nanofluid flow through a circular tube: applicable for use in heat exchangers. Appl Therm Eng. 2018;129:1573–81.
3. Aghakhani S, Pordanjani AH, Karimipour A, Abdollahi A, Afrand M. Numerical investigation of heat transfer in a power-law non-Newtonian fluid in a C-shaped cavity with magnetic field effect using finite difference lattice Boltzmann method. Comput Fluids. 2018;176:51–67.
4. Shahsavar A, Khanmohammadi S, Karimipour A, Goodarzi M. A novel comprehensive experimental study concerned synthesizes and prepare liquid paraffin-Fe_3O_4 mixture to develop models for both thermal conductivity and viscosity: a new approach of GMDH type of neural network. Int J Heat Mass Transf. 2019;131:432–41.
5. Izadi M, Mohebbi R, Delouei AA, Sajjadi H. Natural convection of a magnetizable hybrid nanofluid inside a porous enclosure subjected to two variable magnetic fields. Int J Mech Sci. 2019;151:154–69.
6. Amiri Delouei A, Sajjadi H, Mohebbi R, Izadi M. Experimental study on inlet turbulent flow under ultrasonic vibration: pressure drop and heat transfer enhancement. Ultrason Sonochem. 2019;51:151–9.
7. Liu WI, Alsarraf J, Shahsavar A, Rostamzadeh M, Afrand M, Nguyen TK. Impact of oscillating magnetic field on the thermal-conductivity of water–Fe_3O_4 and water–Fe_3O_4/CNT ferro-fluids: experimental study. J Magn Magn Mater. 2019;484:258–65.
8. Mohebbi R, Izadi M, Sajjadi H, Delouei AA, Sheremet MA. Examining of nanofluid natural convection heat transfer in a Γ-shaped enclosure including a rectangular hot obstacle using the lattice Boltzmann method. Phys A. 2019;526:120831.
9. Afrand M, Esfe MH, Abedini E, Teimouri H. Predicting the effects of magnesium oxide nanoparticles and temperature on the thermal conductivity of water using artificial neural network and experimental data. Physica E. 2017;87:242–7.
10. Yang L, Mao M, Huang JN, Ji W. Enhancing the thermal conductivity of SAE 50 engine oil by adding zinc oxide nano-powder: An experimental study. Powder Technol. 2019;356:335–41.
11. Asadi A, Asadi M, Rezaniakolaei A, Rosendahl LA, Afrand M, Wongwises S. Heat transfer efficiency of Al_2O_3-MWCNT/thermal oil hybrid nanofluid as a cooling fluid in thermal and energy

management applications: an experimental and theoretical investigation. Int J Heat Mass Transf. 2018;117:474–86.
12. Amiri Delouei A, Sajjadi H, Izadi M, Mohebbi R. The simultaneous effects of nanoparticles and ultrasonic vibration on inlet turbulent flow: an experimental study. Appl Therm Eng. 2019;146:268–77.
13. Sajjadi H, Amiri Delouei A, Izadi M, Mohebbi R. Investigation of MHD natural convection in a porous media by double MRT lattice Boltzmann method utilizing MWCNT–Fe_3O_4/water hybrid nanofluid. Int J Heat Mass Transf. 2019;132:1087–104.
14. Mohebbi R, Izadi M, Delouei AA, Sajjadi H. Effect of MWCNT–Fe_3O_4/water hybrid nanofluid on the thermal performance of ribbed channel with apart sections of heating and cooling. J Therm Anal Calorim. 2019;135:3029–42.
15. Sepyani K, Afrand M, Esfe MH. An experimental evaluation of the effect of ZnO nanoparticles on the rheological behavior of engine oil. J Mol Liq. 2017;236:198–204.
16. Shahsavani E, Afrand M, Kalbasi R. Experimental study on rheological behavior of water–ethylene glycol mixture in the presence of functionalized multi-walled carbon nanotubes. J Therm Anal Calorim. 2018;131:1177–85.
17. Ranjbarzadeh R, Akhgar A, Musivand S, Afrand M. Effects of graphene oxide-silicon oxide hybrid nanomaterials on rheological behavior of water at various time durations and temperatures: synthesis, preparation and stability. Powder Technol. 2018;335:375–87.
18. Haq RU, Aman S. Water functionalized CuO nanoparticles filled in a partially heated trapezoidal cavity with inner heated obstacle: FEM approach. Int J Heat Mass Transf. 2019;128:401–17.
19. Saeid NH. Natural convection in a square cavity with discrete heating at the bottom with different fin shapes. Heat Transf Eng. 2018;39:154–61.
20. Chen H-T, Lin M-C, Chang J-R. Numerical and experimental studies of natural convection in a heated cavity with a horizontal fin on a hot sidewall. Int J Heat Mass Transf. 2018;124:1217–29.
21. Hashim I, Alsabery AI, Sheremet MA, Chamkha AJ. Numerical investigation of natural convection of Al_2O_3–water nanofluid in a wavy cavity with conductive inner block using Buongiorno's two-phase model. Adv Powder Technol. 2018;30:399–414.
22. Sheremet MA, Pop I. Effect of local heater size and position on natural convection in a tilted nanofluid porous cavity using LTNE and Buongiorno's models. J Mol Liq. 2018;266:19–28.
23. Khanafer K, AlAmiri A, Bull J. Laminar natural convection heat transfer in a differentially heated cavity with a thin porous fin attached to the hot wall. Int J Heat Mass Transf. 2015;87:59–70.
24. Pordanjani AH, Vahedi SM, Rikhtegar F, Wongwises S. Optimization and sensitivity analysis of magneto-hydrodynamic natural convection nanofluid flow inside a square enclosure using response surface methodology. J Therm Anal Calorim. 2019;135:1–15.
25. Selimefendigil F. Natural convection in a trapezoidal cavity with an inner conductive object of different shapes and filled with nanofluids of different nanoparticle shapes. Iran J Sci Technol Trans Mech Eng. 2018;42:169–84.
26. Pordanjani AH, Aghakhani S, Karimipour A, Afrand M, Goodarzi M. Investigation of free convection heat transfer and entropy generation of nanofluid flow inside a cavity affected by magnetic field and thermal radiation. J Therm Anal Calorim. 2019;137(3):997–1019.
27. Sheikholeslami M, Sajjadi H, Delouei AA, Atashafrooz M, Li Z. Magnetic force and radiation influences on nanofluid transportation through a permeable media considering Al_2O_3 nanoparticles. J Therm Anal Calorim. 2019;136:2477–85.
28. Atashafrooz M, Sheikholeslami M, Sajjadi H, Amiri Delouei A. Interaction effects of an inclined magnetic field and nanofluid on forced convection heat transfer and flow irreversibility in a duct with an abrupt contraction. J Magn Magn Mater. 2019;478:216–26.
29. Mansour MA, Siddiqa S, Gorla RSR, Rashad AM. Effects of heat source and sink on entropy generation and MHD natural convection of Al_2O_3–Cu/water hybrid nanofluid filled with square porous cavity. Therm Sci Eng Prog. 2018;6:57–71.
30. Malik S, Nayak AK. MHD convection and entropy generation of nanofluid in a porous enclosure with sinusoidal heating. Int J Heat Mass Transf. 2017;111:329–45.
31. Ghasemi K, Siavashi M. MHD nanofluid free convection and entropy generation in porous enclosures with different conductivity ratios. J Magn Magn Mater. 2017;442:474–90.
32. Job V, Gunakala S. Unsteady MHD free convection nanofluid flows within a wavy trapezoidal enclosure with viscous and Joule dissipation effects. Numer Heat Transf Part A Appl. 2016;69:421–43.
33. Mehryan SAM, Izadi M, Chamkha AJ, Sheremet MA. Natural convection and entropy generation of a ferrofluid in a square enclosure under the effect of a horizontal periodic magnetic field. J Mol Liq. 2018;263:510–25.
34. Pordanjani AH, Jahanbakhshi A, Nadooshan AA, Afrand M. Effect of two isothermal obstacles on the natural convection of nanofluid in the presence of magnetic field inside an enclosure with sinusoidal wall temperature distribution. Int J Heat Mass Transf. 2018;121:565–78.
35. Bejan A. Entropy generation through heat and fluid flow. Hoboken: Wiley; 1982.
36. Bejan A. Second law analysis in heat transfer. Energy. 1980;5:720–32.
37. Dutta S, Biswas AK, Pati S. Natural convection heat transfer and entropy generation inside porous quadrantal enclosure with nonisothermal heating at the bottom wall. Numer Heat Transf Part A Appl. 2018;73:222–40.
38. Dutta S, Biswas A. Entropy generation due to natural convection with non-uniform heating of porous quadrantal enclosure—a numerical study. Front Heat Mass Transf (FHMT). 2018;10:1–12.
39. Salari M, Kasaeipoor A, Malekshah EH. Three-dimensional natural convection and entropy generation in tall rectangular enclosures filled with stratified nanofluid/air fluids. Heat Transf Res. 2018;49:685–702.
40. Malekpour A, Karimi N, Mehdizadeh A. Magnetohydrodynamics, natural convection, and entropy generation of CuO–water nanofluid in an I-shape enclosure—a numerical study. J Therm Sci Eng Appl. 2018;10:061016.
41. Pordanjani AH, Aghakhani S, Alnaqi AA, Afrand M. Effect of alumina nano-powder on the convection and the entropy generation of water inside an inclined square cavity subjected to a magnetic field: uniform and non-uniform temperature boundary conditions. Int J Mech Sci. 2018;152:99–117.
42. Alnaqi AA, Aghakhani S, Pordanjani AH, Bakhtiari R, Asadi A, Tran M-D. Effects of magnetic field on the convective heat transfer rate and entropy generation of a nanofluid in an inclined square cavity equipped with a conductor fin: considering the radiation effect. Int J Heat Mass Transf. 2019;133:256–67.
43. Karatas H, Derbentli T. Natural convection and radiation in rectangular cavities with one active vertical wall. Int J Therm Sci. 2018;123:129–39.
44. Sheikholeslami M, Li Z, Shamlooei M. Nanofluid MHD natural convection through a porous complex shaped cavity considering thermal radiation. Phys Lett A. 2018;382:1615–32.
45. Lugarini A, Franco AT, Junqueira SLM, Lage JL. Natural convection and surface radiation in a heated wall, C-shaped fracture. J Heat Transf. 2018;140:082501–9.
46. Wang C-H, Feng Y-Y, Yue K, Zhang X-X. Discontinuous finite element method for combined radiation-conduction heat transfer

in participating media. Int Commun Heat Mass Transfer. 2019;108:104287.
47. Feng Y-Y, Wang C-H. Discontinuous finite element method with a local numerical flux scheme for radiative transfer with strong inhomogeneity. Int J Heat Mass Transf. 2018;126:783–95.
48. Sheikholeslami M, Ghasemi A. Solidification heat transfer of nanofluid in existence of thermal radiation by means of FEM. Int J Heat Mass Transf. 2018;123:418–31.
49. Karimipour A. A novel case study for thermal radiation through a nanofluid as a semitransparent medium via discrete ordinates method to consider the absorption and scattering of nanoparticles along the radiation beams coupled with natural convection. Int Commun Heat Mass Transf. 2017;87:256–69.
50. Tighchi HA, Sobhani M, Esfahani JA. Effect of volumetric radiation on natural convection in a cavity with a horizontal fin using the lattice Boltzmann method. Eur Phys J Plus. 2018;133:8.
51. Sobhani M, Tighchi HA, Esfahani JA. Taguchi optimization of combined radiation/natural convection of participating medium in a cavity with a horizontal fin using LBM. Phys A. 2018;509:1062–79.
52. Sheikholeslami M, Seyednezhad M. Simulation of nanofluid flow and natural convection in a porous media under the influence of electric field using CVFEM. Int J Heat Mass Transf. 2018;120:772–81.
53. Sheikholeslami M, Ganji DD. Entropy generation of nanofluid in presence of magnetic field using Lattice Boltzmann method. Phys A. 2015;417:273–86.
54. Vajjha RS, Das DK. Experimental determination of thermal conductivity of three nanofluids and development of new correlations. Int J Heat Mass Transf. 2009;52:4675–82.
55. Maxwell JC, Thompson JJ. A treatise on electricity and magnetism, vol. 2. Oxford: Clarendon; 1904.
56. Brinkman H. The viscosity of concentrated suspensions and solutions. J Chem Phys. 1952;20:571.
57. Patankar S. Numerical heat transfer and fluid flow. Boca Raton: CRC Press; 1980.
58. Krane RJ, Jessee J. Some detailed field measurements for a natural convection flow in a vertical square enclosure. Proc First ASME JSME Therm Eng Joint Conf. 1983;1:323–9.
59. Ghasemi B, Aminossadati S, Raisi A. Magnetic field effect on natural convection in a nanofluid-filled square enclosure. Int J Therm Sci. 2011;50:1748–56.